

Design Optimization of Soft-Contact Freestanding Rotary Triboelectric Nanogenerator for High-Output Performance

Junhuan Chen, Xuelian Wei, Baocheng Wang, Ruonan Li, Yanggui Sun, Yating Peng, Zhiyi Wu,* Peng Wang,* and Zhong Lin Wang*

The soft-contact freestanding rotary triboelectric nanogenerator (FR-TENG), with the capabilities of high output performance and excellent efficiency, presents interesting applications in driven nonequilibrium plasma jets, mass spectrometry, electrospinning, and so on. For enhancing the output performance of FR-TENG, detailed and in-depth research focusing on the design method is discussed in this paper, mainly consisting of the following four parts: 1) design reasonable geometric structure, 2) select triboelectric layers, 3) choose a reasonable signal acquisition, and 4) investigate influencing factors. Benefiting from this four-step systematic research, a modified FR-TENG with better output performance is successfully constructed. A corresponding open-circuit voltage density of $1.27 \times 10^5 \text{ V m}^{-2}$ is achieved, which is over two-fold higher compared to the largest one among the previous similar articles. Therefore, the four-step systematic research is demonstrated to remarkably enhance the output performance of the soft-contact FR-TENG. This work not only presents a modified FR-TENG with ultrahigh voltage density that inhibits bacterial corrosion, enables high-voltage electrostatic dust removal, and enables impressive current cathodic protection of marine pipelines and urban buried pipelines, but also can be regarded as guidance for the design of soft-contact FR-TENG.

development.^[3] As a new energy harvesting invention^[4] with great potential application value,^[5] triboelectric nanogenerator (TENG) has gradually advanced,^[6] whether in theoretical research, structural innovation, or application development, since its discovery in 2012,^[7] which has four main applications nowadays: micro-nanoenergy,^[8] self-powered sensor,^[9] blue energy,^[10] and high-voltage application.^[11] Different from the low-voltage characteristic of the electromagnetic generator, TENG can be considered as a current source^[12] with high voltage and low current output characteristics. Therefore, the research on the high-voltage application scenarios and mechanism of TENGs is gradually receiving extensive attention from researchers.^[13]

Lin et al. designed a TENG with a radially distributed disk structure for the first time, which opens up many novel structures and potential applications.^[14] Then, a freestanding rotary triboelectric nanogenerator (FR-TENG) with radial arrays of microsized sectors was designed, which achieved multiple charge transfer and generated higher short-circuit current (I_{SC}).^[15] FR-TENG has received widespread attention due to its characteristics of higher open-circuit voltage (V_{OC}) and short-circuit current.^[16] However, since the conventional FR-TENG


1. Introduction

The development of sustainable energy^[1] and the improvement of energy utilization^[2] have become important issues related to the industrialization of the world and economic

J. Chen, X. Wei, B. Wang, R. Li, Y. Sun, Y. Peng, Z. Wu, Z. L. Wang
Beijing Institute of Nanoenergy and Nanosystems
Chinese Academy of Sciences
Beijing 100083, P. R. China
E-mail: wuzhiyi@binn.cas.cn; zhong.wang@mse.gatech.edu

J. Chen, Y. Peng, P. Wang
Key Lab of Marine Environmental Corrosion and Biofouling
Institute of Oceanology
Chinese Academy of Sciences
Qingdao 266071, China
E-mail: wangpeng@qdio.ac.cn

J. Chen, Y. Peng, P. Wang
Open Studio for Marine Corrosion and Protection
Pilot National Laboratory for Marine Science and Technology (Qingdao)
168 Wenhai Middle Road, Qingdao 266237, China

 The ORCID identification number(s) for the author(s) of this article can be found under <https://doi.org/10.1002/aenm.202102106>.

J. Chen, Y. Peng
School of Earth and Planetary
University of Chinese Academy of Science
Beijing 100049, China

X. Wei, B. Wang, Z. Wu, Z. L. Wang
College of Nanoscience and Technology
University of Chinese Academy of Science
Beijing 100049, China

Z. Wu, Z. L. Wang
CUSTech Institute
Wenzhou 325024, China

Z. L. Wang
School of Materials Science and Engineering
Georgia Institute of Technology
Atlanta, GA 30332-0245, USA

DOI: 10.1002/aenm.202102106

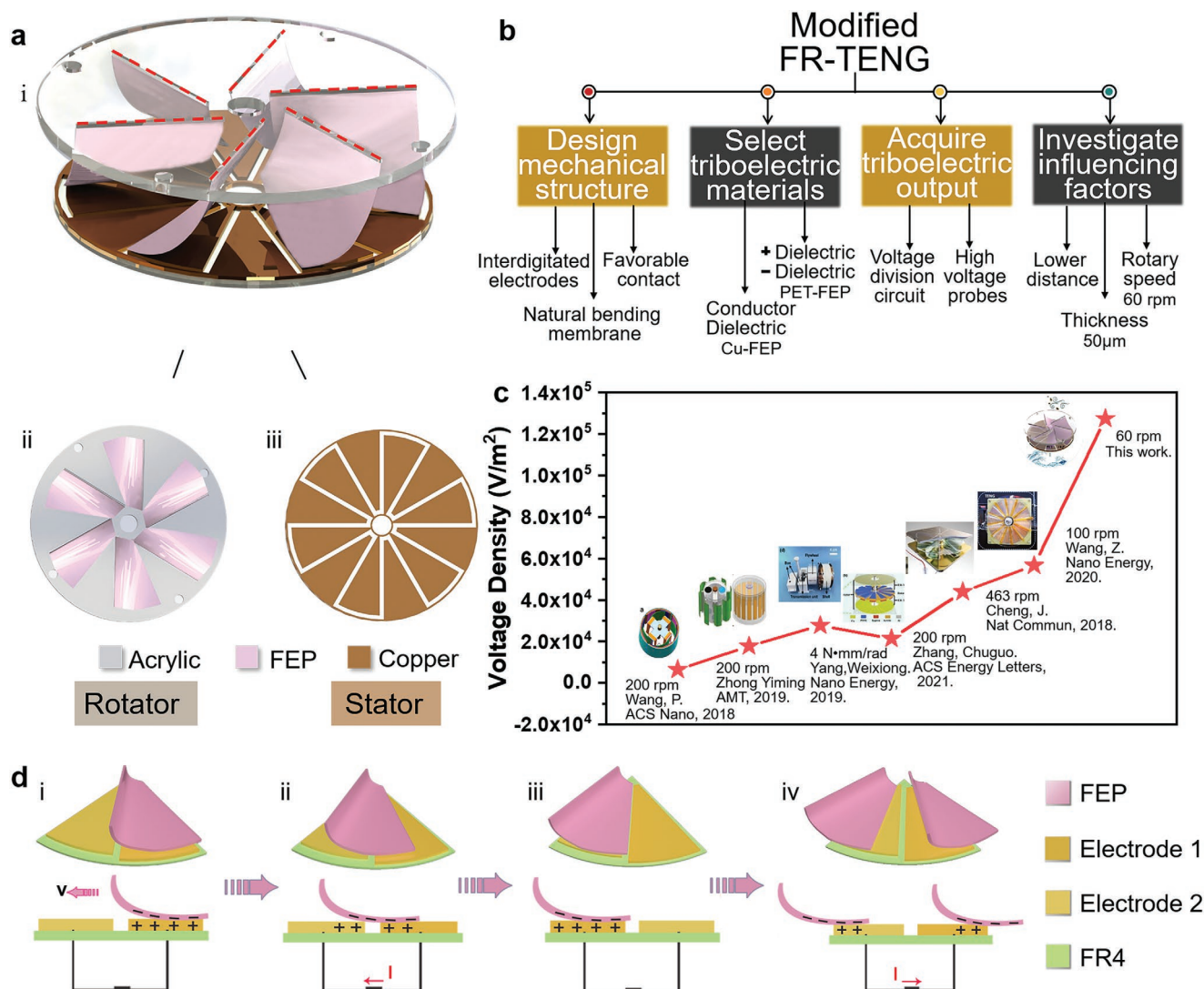


Figure 1. The structure and working principle of the modified FR-TENG. a) The structure photos of the modified FR-TENG, a rotator, and a stator. b) The structural frame of the systematic research of the modified FR-TENG. c) Comparison of open-circuit voltage density between this paper and other similar articles. Reproduced with permission.^[17] Copyright 2018, American Chemical Society. Reproduced with permission.^[18b] Copyright 2019, John Wiley and Sons. Reproduced with permission.^[19a] Copyright 2019, Elsevier. Reproduced with permission.^[18c] Copyright 2021, American Chemical Society. Reproduced with permission.^[18a] Copyright 2018, Springer Nature. Reproduced with permission.^[13c] Copyright 2020, Elsevier. d) The general working principle of the modified FR-TENG.

composed of two hard disks faces problems of serious abrasion and short service lifespan, the soft-contact TENG has been introduced.^[17] Compared with the conventional sliding friction structure, the soft-contact FR-TENG with higher V_{OC} of up to kilovolts is easy to collect energy, especially low-frequency energy, on account of weak friction resistance.^[18] Due to the electrostatic attraction, the positive triboelectric dielectric could contact the negative triboelectric dielectric closely, which further increases the triboelectric output.^[13c,19] From previous articles and books, we can conclude that the geometric structure, effective contact area, collocation of dielectric materials and surrounding environmental factors and so on, have a significant impact on the triboelectric output of FR-TENG. However, none of these studies have been focused on the normalizing design of FR-TENG and could be regarded as a reference, which is indispensable for improving the output performance and advancing application.

For the formation of systematic design guidance on soft-contact FR-TENG, detailed and in-depth research is carried out firstly, mainly consisting of the following four parts: 1) design reasonable geometric structure according to the specific application requirement, such as high voltage or large current, 2) select triboelectric layers with better triboelectric properties and mechanical properties, 3) choose a reasonable signal acquisition, and 4) investigate influencing factors in consideration of the application environment. Considering the above four processes elaborately, the output performance of the modified FR-TENG is remarkably enhanced. This four-step systematic research has been demonstrated to effectively raise the triboelectric properties (**Figure 1a–c**). Most noteworthy, a corresponding open-circuit voltage density can be improved to $1.27 \times 10^5 \text{ V m}^{-2}$, retaining the largest one compared with previously reported works based on the soft-contact

FR-TENG. An accelerated wear test at 600 rpm was first used to demonstrate the wear resistance and durability of the modified FR-TENG in positive dielectric–negative dielectric mode. Due to its high output performance, this modified FR-TENG will play an effective role in the inhibition of microbial corrosion, high-voltage electrostatic dust removal scenarios, impressed current cathodic protection (ICCP) in marine environments and urban buried pipelines. In addition, high voltage electrostatic breakdown can generate between one electrode of the grounding modified FR-TENG and an external grounding conductor. Thus, the externally grounding conductor can harvest energy well through the durative electrical spark discharge and arc discharge which are not anymore restricted between positive and negative electrodes. This work has a crucial significance for boosting the output performance, and could provide specific and detailed guidance for design optimization of the soft-contact FR-TENG, and also offers a reference for other TENGs.

2. Experimental Section

2.1. Method

In order to raise the output performance of the FR-TENG, a systematic study was carried out and divided into the following sections (Figure 1b).

2.1.1. Design Mechanical Structure

To achieve high voltage, the reasonable geometric structure of FR-TENG, the unit of interdigitated electrode, and the shape of fluorinated ethylene propylene (FEP) films were tailoring. The relative position between FEP films and interdigitated electrode was explored. The structure of the modified FR-TENG is shown in Figure 1a. The rotor is composed of flexible films and acrylic substrate. The interdigitated electrode made of the printed circuit board (PCB) is used as the stator.

2.1.2. Select Triboelectric Materials

Considering the triboelectric sequence^[20] and the properties of machinery and chemistry, the output performance of the diverse triboelectric dielectrics with different operating modes was compared. These dielectric layers are made by commercial mature production technology, to promote the commercial application of FR-TENG. Initially, the conductor–dielectric mode was chosen. FEP film was selected as the negative triboelectric layer, and copper (Cu) was selected as the positive triboelectric layer and charge-transport electrode. Finally, referring to the triboelectric sequence and the chemical groups of the various triboelectric dielectrics, the positive dielectric–negative dielectric mode was chosen as the most efficient mode. In this mode, polyethylene terephthalate (PET) films act as the positive triboelectric dielectric, and FEP films act as the negative triboelectric dielectric, showing promising output performance.

2.1.3. Acquire Triboelectric Output

According to the basic output characteristics of TENG, a reasonable signal acquisition mode should be chosen to accurately represent the output performance of TENG. 6514 electrometer reasonable test range: current measurement: <1 fA (containing noise) \approx 20 mA; voltage measurement: 10 μ V (digital resolution limit, containing noise) \approx 200 V; charge measurement: 10 fC (digital resolution limit, containing noise) \approx 20 μ C. When FR-TENG was tested first, the triboelectric output reached about 360 V, 200 nC, 5 μ A, in which the voltage was beyond the test range of 6514 electrometer, which would make the measurement inaccurate. Referring to the high open-circuit voltage of the modified FR-TENG and the range of Keithley 6514 electrometer, Voltage Division Circuit combined with Keithley 6514 electrometer and High Voltage Probes combined with Digital Oscilloscope were used to measure the open-circuit voltage. Keithley 6514 electrometer was also used to measure the I_{SC} and Q_{SC} of the modified FR-TENG.

2.1.4. Investigate Influencing Factors

For better application of the modified FR-TENG in a real environment, several key parameters, such as the unit and materials of interdigitated electrodes, processing techniques of films, the distance between rotor and stator, the thickness of triboelectric layer, and rotary speed should be taken into consideration.

Due to the discharge phenomenon that could improve the output voltage, the modified FR-TENG can act as a high voltage power source. A spark discharge and an arc discharge appear persistently between the externally grounding conductor and the electrode of the grounding modified FR-TENG, so the externally grounding conductor could obtain electric energy converted from mechanical energy through the modified FR-TENG.

2.2. Experiment

The Q_{SC} of triboelectric nanogenerator can be calculated by^[14,15,21]

$$Q_{SC} = \frac{S\sigma x}{d_0 + x} \quad (1)$$

where Q_{SC} is the transferred charges, S is the contact area, σ represents the triboelectric charge density, x represents the sliding distance and d_0 is the thickness of the dielectric layer. The polarized charge density and transferred charge density have a differential impact on the output performance and output stability of a TENG. And the contact area between the triboelectric dielectrics directly affects the polarized charge density. In state i and state iii (Figure 1d), the contact area between the interdigitated electrode and the soft film must be the same. To obtain the contours of interdigitated electrode 1 and electrode 2, the dashed line that coincides with the center of the chassis, is transformed by Equilong Transformation in different directions in SolidWorks software (Figure S1a, Supporting

Information). And the blue area is the contact area between the soft films and the electrodes, after a single cycle of rotor movement (Figure S1a, Supporting Information). A different unit of interdigitated electrodes was designed by SolidWorks software and manufactured by commercially available PCB technologies. The diameter and thickness of the stator are 100 and 1.5 mm, respectively. The distance between electrode 1 and adjacent electrode 2 is 2 mm. The rotator consisted of naturally curved cast FEP films (ZY-0.05, ZeYou, China) and an acrylic substrate. The acrylic substrate (110 mm in diameter and 2.5 mm in thickness) was connected to the Rotating Motor (86HSE8N, PFDE, China) by screws and nuts. In order to fix FEP films well, Laser Beam Cutting Machine (6090, 31 Degree Technology, Jiaxing, China) was used to slot on the acrylic substrate. For obtaining an optimal contact state between the curved FEP films and the interdigitated electrodes, the relative position between the slot and the interdigitated electrode was adjusted time and time again. Meanwhile, the shape of FEP films would be modified with the relative position changing. As illustrated in Figure S1b of the Supporting Information, ideally, the end of FEP film contacting with the interdigitated electrodes is in the contact position of FEP distal end position (the yellow dotted line). The other end of the FEP film is fixed on the slot of the acrylic substrate. The distance between the rotator and the stator should be considered when designing the shape of FEP film. With continuous adjustments, contact states can be divided into three types: Over-Contact, Less-Contact, and Favorable-Contact. When the effective contact area of soft-contact FR-TENG is larger than that of electrode 1, the triboelectric layers will simultaneously contact electrode 1 and electrode 2 always time during rotation, resulting in that the potential difference cannot reach the optimal value. When the effective contact area is less than that of electrode 1, the electrode area cannot be fully utilized and the triboelectric output will also decrease. The case A and B are Over-Contact state. The case C, the conventional contact state in other articles, is Less-Contact state. From Figure S1b (ii) of the Supporting Information, after further adjustment based on case C, other cases come up: case C+5 mm, case C+3 mm, and case D. The effective contact area of case D with the interdigitated electrode is close to that of electrode 1 (Table S1, Supporting Information). As the effective contact area of case D is almost the same as the area of electrode 1, the output performance of it is the best compared to the other cases, so case D could be regarded as the Favorable-Contact state. The corresponding photos of these cases of modified FR-TENG are shown in Figure S2 of the Supporting Information.

Electrometer (6514, Keithley, USA), National Instruments (National Instruments, Cleveland, OH, USA), LabVIEW System (National Instruments, Cleveland, OH, USA), and Digital Storage Oscilloscope (InfiniiVision DSOX2024A, KEYSIGHT, USA) with High Voltage Probes (10076C, KEYSIGHT, 66.7 M Ω , 1/100) were used to measure triboelectric output signs (V_{OC} , I_{SC} , Q_{SC}) of the modified FR-TENG. The surface morphology of dielectric films was characterized by scanning electron microscope (SEM) (SU8010, Hitachi) and atomic force microscope (MFP-3D, OXFORD). The temperature and humidity chamber (Y-HD-150L, Aerospace Zhida) was used to explore the influence of temperature and relative humidity on triboelectric output independently.

3. Results and Discussion

3.1. Working Principle

Considering the wireless moving object, the freestanding triboelectric-layer mode was chosen to improve the triboelectric output property. The four photos (i \rightarrow ii \rightarrow iii \rightarrow iv) briefly illustrate the operating mechanism of the modified FR-TENG (Figure 1d). In the initial state, electrode 1 of interdigitated electrodes is covered with FEP films in a floating structure. By the coupling of the triboelectrification and electrostatic induction, negative charges generated on the FEP films are equivalent to the positive ones on the copper. Under the influence of pulling force and electrostatic attraction, the soft FEP films of the rotator create a relative rotation between the different fractions of interdigitated electrodes gradually. The charges will be redistributed between electrode 1 and electrode 2 due to the electrostatic equilibration. Therefore, the free electrons flow from electrode 2 to electrode 1 in an external circuit (ii), finally reach equilibrium (iii). As rotation again, the free electrons will flow back in opposite-direction (iv), until reaching a new equilibrium (i). The triboelectric output with the alternating current characteristic is generated by the periodical charge transfer.

3.2. Output Performance

As shown in Figure 2, the different contact conditions have various implications on the output performance of the modified FR-TENG. FEP films' shape on the rotator and their relative positions with interdigitated electrodes were changed again and again to achieve optimal contact and increase the triboelectric output. In comparison with the triboelectric output property of the Favorable-Contact state (Figure 3a; Figure S3a,b, Supporting Information), Less-Contact and Over-Contact states result in poor triboelectric output.

The cases of A and B are Over-Contact case in which the FEP films always contact electrode 1 and electrode 2 of the interdigitated electrode. It is obvious that the open-circuit voltage magnitudes in these two cases are lower than that of case C. As a conventional contact condition of FR-TENG, case C has a less effective contact area. Case D in the optimal contact state has a first-rank triboelectric output (Figure 3a). The peak-to-peak V_{OC} , Q_{SC} , and I_{SC} of case D are about 550 V, 240 nC, and 7 μ A, respectively, at 60 rounds per minute (rpm).

The distance between rotator and stator directly affects the triboelectric output (Figure 3b; Figure S4a, Supporting Information). The Q_{SC} progressively augments to 230 nC as the distance decreases. But the V_{OC} achieves a maximum, 540 V, at 3 mm. To achieve a favorable contact state, the optimal length of the corresponding FEP film should be changed when altering the distance.

The influence of the unit of interdigitated electrodes on the triboelectric properties has been tested. As illustrated in Figure 3c and Figure S3c,d (Supporting Information), the V_{OC} of 3 units is up to 1000 V. And the I_{SC} of 8 units is up to 10 μ A. With the multiplication of units, the effective contact area decreases, minimizing the V_{OC} gradually. Conversely, the

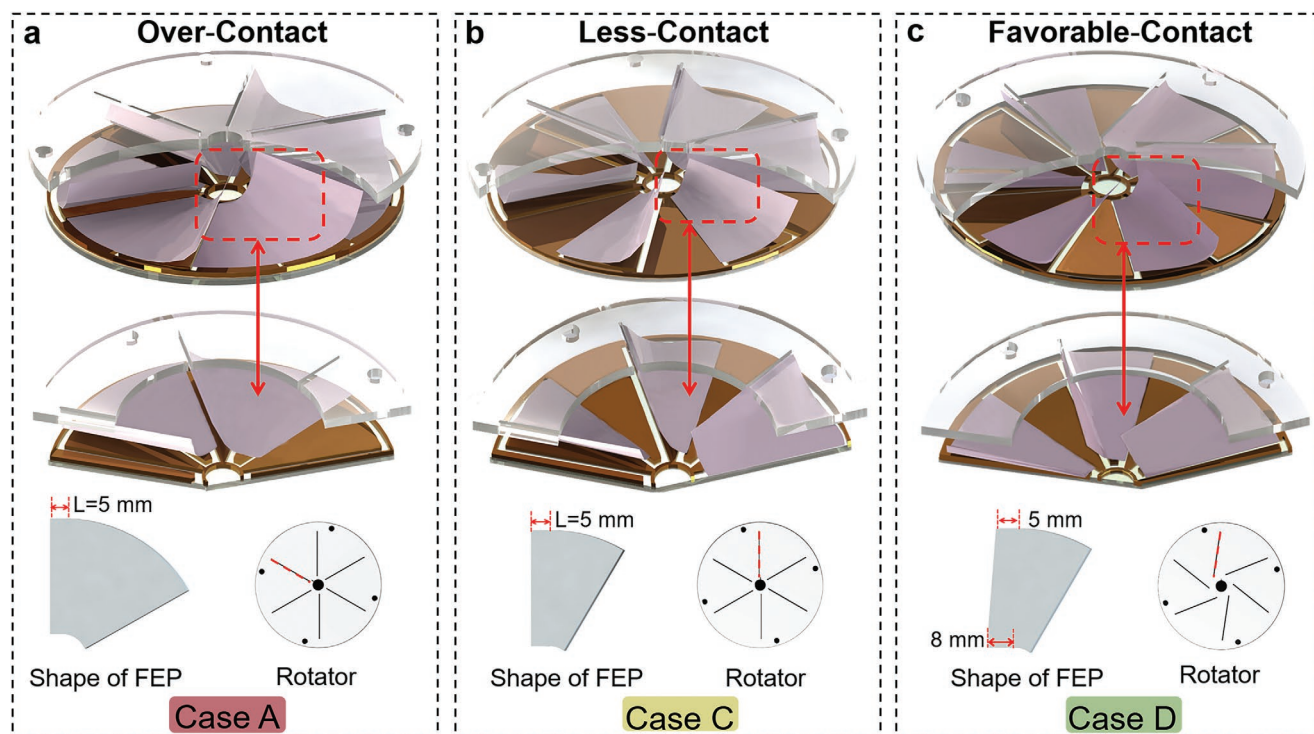


Figure 2. Photo of simulated contact state of the modified FR-TENG with special shapes of film and the different relative positions between the rabbit on the rotator and interdigitated electrodes. a) Photo of simulated contact state of case A. b) Photo of simulated contact state of case C (the conventional contact state of FR-TENG). c) Photo of simulated contact state of case D.

time course of charge transfer decreases, and the I_{SC} gradually increases, referring to the formula

$$I = dQ/dt \quad (2)$$

But when the unit of interdigitated electrodes is further reduced, the I_{SC} decreases significantly, due to the dramatic lowering of the amounts of transferred charges.

The rotator with a metallic conductor placing on it was slightly tilted and was not concentric with the stator. The metal conductor can only contact the interdigital electrode per rotation, and once spark discharge was generated, which is defined as the one-point discharge. Influenced by the one-point discharge, the modified FR-TENG has shown the double V_{OC} compared with that without discharge (Figure 3d). The peak-to-peak open-circuit voltage of case D influenced by one-point discharge has increased to 1060 V. The center of the specially designed 6' units structure with fan-shaped spacing, has multiple tips. When the rotator rotated, some spark discharges occurred between the multiple tips continuously, which is defined as multipoints discharges. Experimental data shows that the V_{OC} of one-point discharge condition is relatively higher than that of multipoint discharges condition. It proves that mechanical design can enhance the charge accumulation and further boost the output performance of TENG.

One of the advantages of TENG is wide material selections. The dielectric property of the triboelectric layer has a great influence on the electrical output.^[22] By combining different materials with opposite tribopolarity, the output performance of TENG can be further improved. The cooperation of materials is

categorized into two kinds: conductor–dielectric mode and positive dielectric–negative dielectric mode. In conductor–dielectric mode, the conductor, such as Cu and Al, must act as both the triboelectric dielectric and the charge transfer electrode. In the positive dielectric–negative dielectric mode, metal or metal oxide shall be only used as the electrode. In **Figure 4a–c**, in conductor–dielectric mode, the peak-to-peak V_{OC} , Q_{SC} , and I_{SC} of the modified FR-TENG made of FEP films and Cu reach a higher value, about 550 V, 280 nC, and 10 μ A. The triboelectric output of the modified FR-TENG made of PET films and FEP films reach a relatively highest output, about 650 V, 550 nC, and 21 μ A, respectively. Unconventionally, the cooperation of FEP films and PET films get a better output performance, even though both FEP films and PET films are of a relatively negative position in the triboelectric sequence. That may be attributed to closer contact in the cooperation of FEP films and PET films with high permittivity, as triboelectrification and electrostatic induction will be increased by closer contact. In Table S2 of the Supporting Information, the thicknesses, area, flexure strength, flexural modulus, coefficient of static friction, Poisson's ratio, permittivity, and manufacturer of these commercial dielectric layers are shown.

Considering the chemical property and the output performance of these materials, we can find that materials with negative groups possess better triboelectric properties (Figure 4d). The $-F$ halogen and $-CO-$ group could enhance the electron density on the surface of dielectrics. The $-CH_2-$, $-NH-$, and $-COO-$ group will decrease the electron clouds density on the surface of dielectrics.^[23] There are numerous $-F$ halogen groups on the chemical structure of FEP film, and $-COO-$ groups on

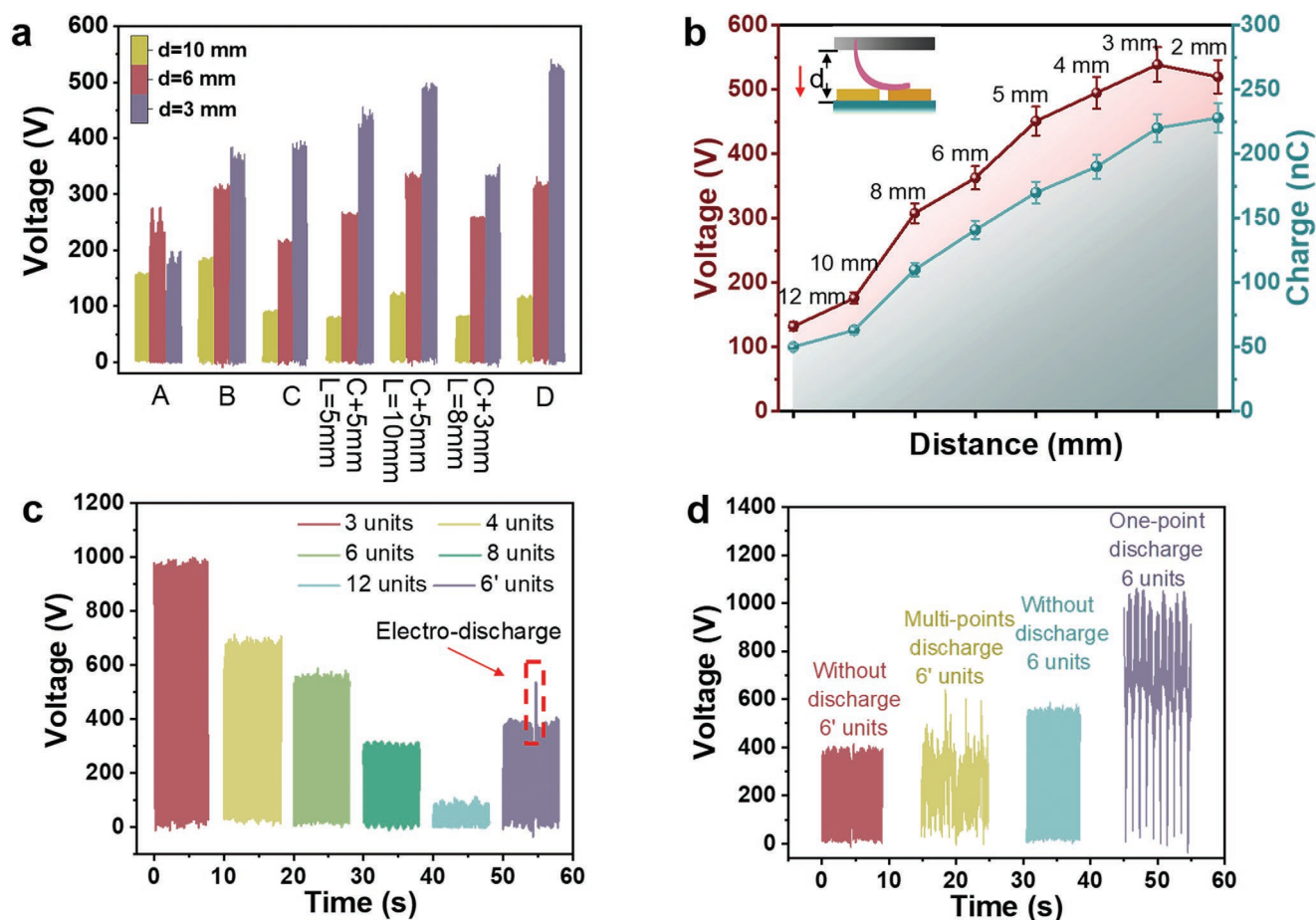


Figure 3. The output performance of the modified FR-TENG is influenced by different contact conditions. a) The triboelectric output of the modified FR-TENG at different FEP shapes and positions. b) The influence of the different distances between stator and rotor to the modified FR-TENG. c) The open-circuit voltage of the modified FR-TENG at the different units of interdigitated electrodes. d) One-point discharge and multipoints discharge situation impact the output performance of the modified FR-TENG.

the chemical structure of PET film, so a relatively higher triboelectric output can be obtained. Results infer that by modifying the chemical structure of functional groups of triboelectric layers, the output performance of TENG can be improved.

In Figure 4e, the two different processing techniques of FEP films show differential output performances. The modified FR-TENG with cast FEP films has better triboelectric output than that with blown FEP films. The peak-to-peak V_{OC} and Q_{SC} of this modified FR-TENG with cast films reach 450 V, 190 nC. While the V_{OC} and Q_{SC} of the modified FR-TENG with FEP films fabricated from the blown molding process are relatively lower, about 330 V and 110 nC. The surface morphology of blown film (i) and cast film (ii) were characterized by SEM (Figure 5a). More small voids exist on the surface of cast films, which increase the specific surface areas, and improve the triboelectric output. Thus, in the subsequent experiments, FEP cast films are selected as the negative triboelectric dielectric. Namely, the advanced processing technology of dielectric is able to facilitate the increase of the output performance of TENG.

An accelerated wear test was used to test the wear resistance and durability of the modified FR-TENG in positive dielectric (PET)–negative dielectric (FEP) mode. Meanwhile, during

the accelerated wear test, we monitored the change of ambient temperature and humidity. We also used the Temperature and Humidity Chamber to explore the influence of temperature and relative humidity on triboelectric output independently (Figure S4b,c, Supporting Information). Temperature and relative humidity have a certain effect on the output performance of the modified FR-TENG in the measuring range. And the influence of relative humidity has slightly heavier than that of temperature. After 6 days of the accelerated wear test at 600 rpm, the peak-to-peak open-circuit voltage drops slightly from 610 to 560 V (Figure 4f). And the modified FR-TENG is more sensitive to the humidity of the test environment. The V_{OC} gradually decreases as the environmental humidity increases. Yet when the ambient humidity returned to a normal level, the open-circuit voltage gradually increases. The modified FR-TENG composed of PET films and FEP films has better abrasion resistance, and the output performance also has a certain stability. As depicted in Figure 5b, after six days of accelerated wear test, slight wear occurs on the surface of FEP film (i → iii) and PET (ii → iv) film in this modified FR-TENG. From the stereomicroscope images in Figure S5 of the Supporting Information, an increase in surface roughness can be found after the accelerated wear test.

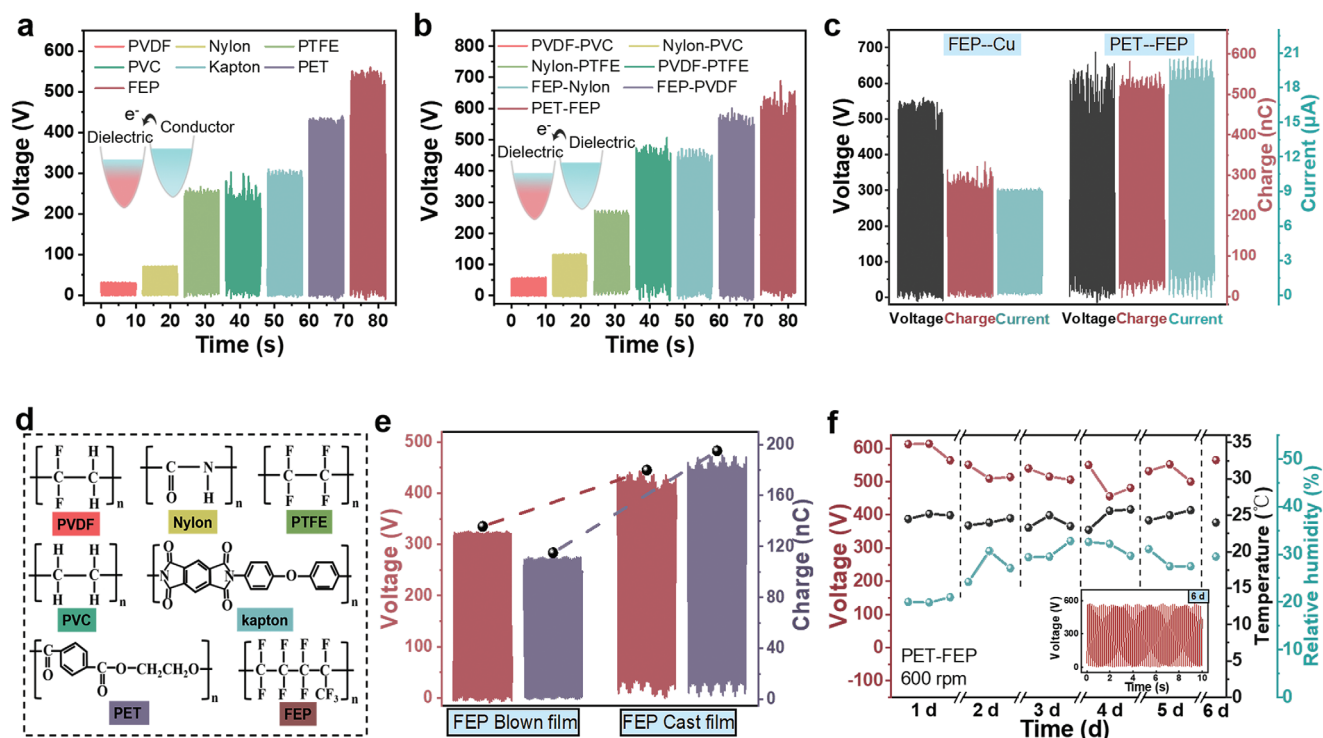


Figure 4. The output performance of the modified FR-TENG is influenced by a variety of dielectric materials. a) The open-circuit voltage of the modified FR-TENG in dielectric–conductor mode. b) The open-circuit voltage of the modified FR-TENG in negative dielectric–positive dielectric mode. c) Comparison of the triboelectric output of the two modified FR-TENG with different cooperation of dielectric. d) Chemical structures of the triboelectric materials. e) The open-circuit voltage and transferred charge of the modified FR-TENG influenced by different manufacturing techniques of FEP films. f) Stability and wear resistance test of the modified FR-TENG by the accelerated wear test.

Most triboelectric dielectrics are polymer materials. These triboelectric dielectrics with unsaturated double bonds, branched chains, carbonyl groups, etc., are easy to age. The bond energy of C–F is greater than that of the C–H bond, playing a significant role in protecting the carbon chain,^[24] so FEP films and polytetrafluoroethylene (PTFE) films have better aging resistance. FEP films and PTFE films are often chosen as triboelectric dielectric due to their better triboelectric properties and aging resistance. Polyester film has ester groups more prone to age. By improving the quality of films through advanced processing polymerization methods, the antiaging features of the triboelectric dielectric will be enhanced. Therefore, the polarized charge durability and the stability of triboelectric output will be improved accordingly.

Figure 5c shows the equivalent circuit of TENG coupled with high resistance R_1 (10 G Ω) and R_2 (1 G Ω). The peak-to-peak V_{OC} of the modified FR-TENG is calculated by the principle of voltage distribution

$$V_{OC} = R_1 V / R_2 \quad (3)$$

One end of the external grounding conductor is close to but not in contact with electrode 1 of the modified FR-TENG whose electrode 2 is grounded. Spark discharge occurred between the external conductor and electrode 1 at 60 rpm (Figure 5d). When the rotary speed increases to 600 rpm, more intense spark discharge and arc discharge occur instantly between the external conductor and electrode 1, which is not anymore

limited between the positive and negative electrodes of TENG. It is proved again that, as the rotary speed increases, the peak-to-peak open-circuit voltage and the short-circuit current will improve accordingly. As the rotator continues to rotate, spark discharge and arc discharge persist. And the equivalent circuit of the modified FR-TENG coupled with an external conductor is shown in Figure 5c (ii). The persistent spark discharge and arc discharge are illustrated in Videos S1 and S2 of the Supporting Information.

The internal resistance of Al is relatively higher than Cu, resulting in higher open-circuit voltage, lower short-circuit current, and less amount of transferred charge (Figure 5e). Although the Al electrode is more positive than Cu in the triboelectric sequence, the transferred charge between Al interdigitated electrodes is inferior to Cu. This result can be attributed to that the Al electrode is easily oxidized to Al_2O_3 in the natural environment.

The theoretical formula of Q_{SC} of triboelectric nanogenerator represented by (1), proves the linear negative correlation between the output performance and thickness (d_0) of the dielectric layer. The FEP films are subjected to two beneficial forces: pulling force that causes the films to slide over the interdigitated electrode; electrostatic attraction force that keeps the films close to the surface of interdigitated electrode tightly (Figure 5f,g). When the FEP film thickness is 30 μm , the V_{OC} and Q_{SC} are lower, about 260 V and 100 nC. It is found that under the pulling force of the rotating motor, the head of FEP film was pulled up, not contacting the Cu electrode anymore. The rapid decrease of

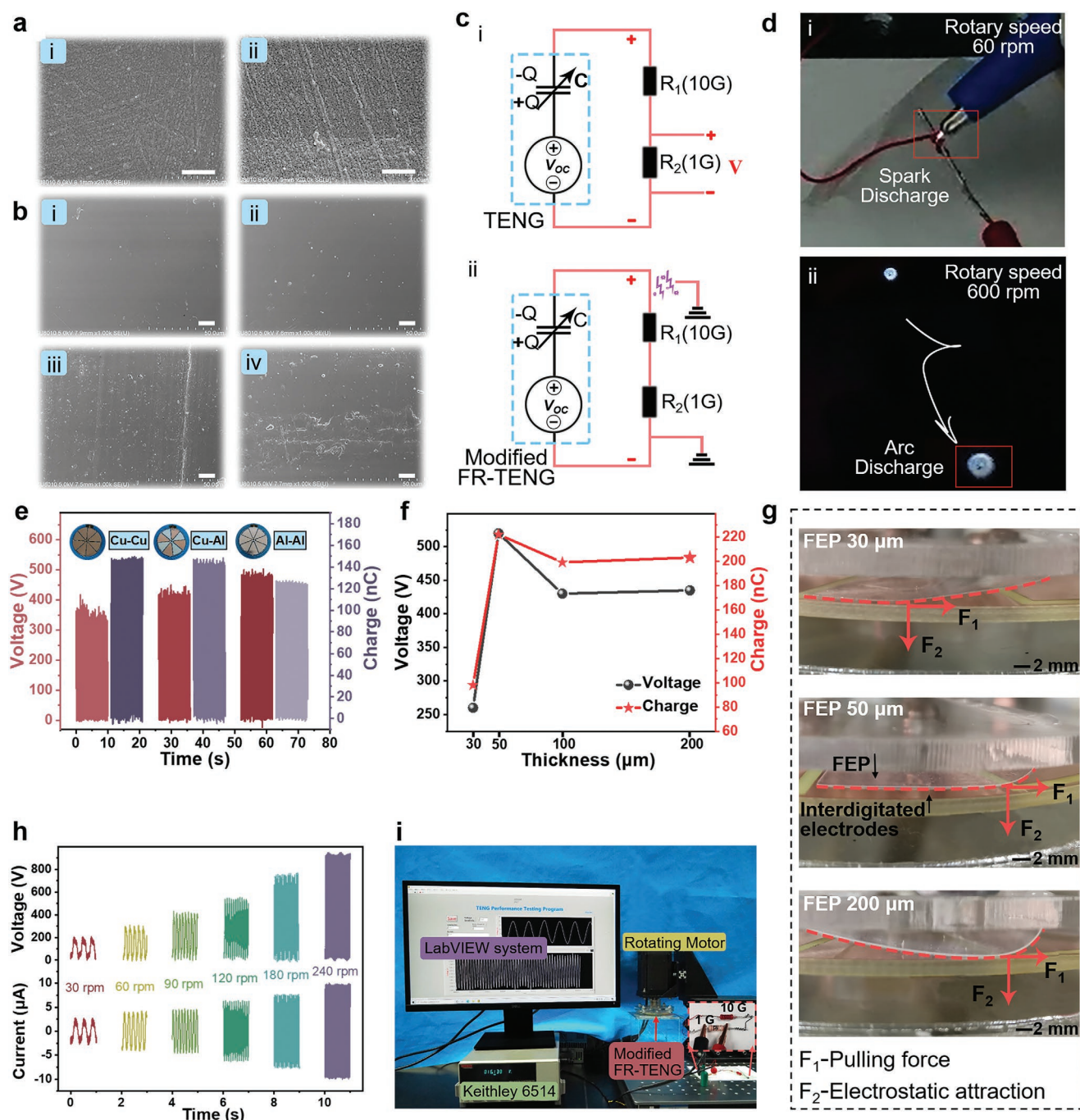


Figure 5. SEM image of surface morphology of dielectric films, and different effects on the triboelectric output. a) SEM image of surface morphology of blown film (i) and cast film (ii) of FEP (Scale bar: 1 μm). b) SEM image of surface morphology of FEP (i \rightarrow iii) and PET (ii \rightarrow iv) before and after Accelerated Wear Test. (scale bar: 10 μm). c) Photo of the equivalent circuit of triboelectric nanogenerator coupled with higher resistance R_1 and R_2 (i), and the equivalent circuit of the modified FR-TENG with an external conductor, generating spark discharge and arc discharge (ii). d) The spark discharge in the experiment at 60 rpm (i), and the arc discharge in the experiment at 600 rpm (ii). e) The output performance of the modified FR-TENG influenced by different materials of interdigitated electrodes. f) The V_{OC} and the Q_{SC} of the modified FR-TENG at different thicknesses. g) Different contact states between 30, 50, 200 μm FEP films and 6 units interdigitated electrodes. h) The V_{OC} and I_{SC} of the modified FR-TENG at different rotating speeds. i) The static photo of the working status of the final modified FR-TENG.

effective contact area reduces the triboelectric output. The V_{OC} and Q_{SC} of modified FR-TENG with FEP films in 50 μm thickness reach the best output performance, about 530 V and 222 nC. With the increase in the thickness of FEP film, the effect of

triboelectrification coupling with electrostatic induction is diminished, which would decrease the output. And the tail of thicker FEP film is easy to bend and warp, which reduces the effective contact area and further decreases the output performance.

The V_{OC} and I_{SC} of 6 units modified FR-TENG at diverse rotary speeds were tested (Figure 5h). The V_{OC} and I_{SC} of the modified FR-TENG increase linearly with the acceleration of the rotating motor. Different from the common FR-TENG, the V_{OC} of the modified FR-TENG obviously increases as the rotational speed improved. This unusual characteristic may be attributed to that gradually increasing centripetal force that changes the direction of dielectric layers. And the effective contact area between different triboelectric polarity dielectric is maximized, thereby increasing the open-circuit voltage. As the acceleration of rotary speed, the time course per cycle of charge transfer is decreased. And the short-circuit current gradually increases, referring to the formula (2). The working status of the final modified FR-TENG is shown in Figure 5i and Video S3 (Supporting Information).

4. Conclusions

Here, systematic research of soft-contact FR-TENG has been demonstrated, which could be deemed guidance for the normalizing design of it, aiming to optimize the structure of soft-contact FR-TENG for high-output performance. This systematic research has been proved to effectively improve the triboelectric output of soft-contact FR-TENG, and also adapts to other triboelectric nanogenerators, mainly consisting of the following four parts: 1) design reasonable geometric structure for high voltage,

2) select triboelectric layers with better triboelectric properties and mechanical properties, 3) choose a reasonable signal acquisition, and 4) investigate influencing factors in consideration of the application environment. Benefiting from the four-step systematic research, the modified FR-TENG with better output performance is finally proposed. In order to achieve better triboelectric output performance, Over-Contact state and Less-Contact state should be avoided. Case D ($d = 3$ mm) achieved a Favorable-Contact state, and the triboelectric output could reach 550 V, 240 nC, and 7 μ A. The effective contact area of the 3 units modified FR-TENG is higher than that of other units, so the output voltage of it is higher, up to 1000 V. At the same time, the discharge can increase the output performance of the modified FR-TENG, and the V_{OC} of one-point discharge is higher than multipoints discharge, about 1060 V. Then the influence of various materials, different processing technologies, and cooperation modes have been tested. In addition, we explored the role of chemical bonds of triboelectric materials. The triboelectric output of this modified FR-TENG with PET (50 μ m) and cast FEP film (50 μ m) reached 650 V, 550 nC, and 21 μ A. The influential factors of distance, thickness, and rotary speed were also investigated. The modified FR-TENG in case D, consisting of 6 units of interdigital electrode, PET films (50 μ m), and FEP films (50 μ m), in 3 mm distance, has better triboelectric output performance and wear resistance after the Accelerated Wear Test at 600 rpm. And in this modified FR-TENG, spark discharge and arc discharge occur instantly between the

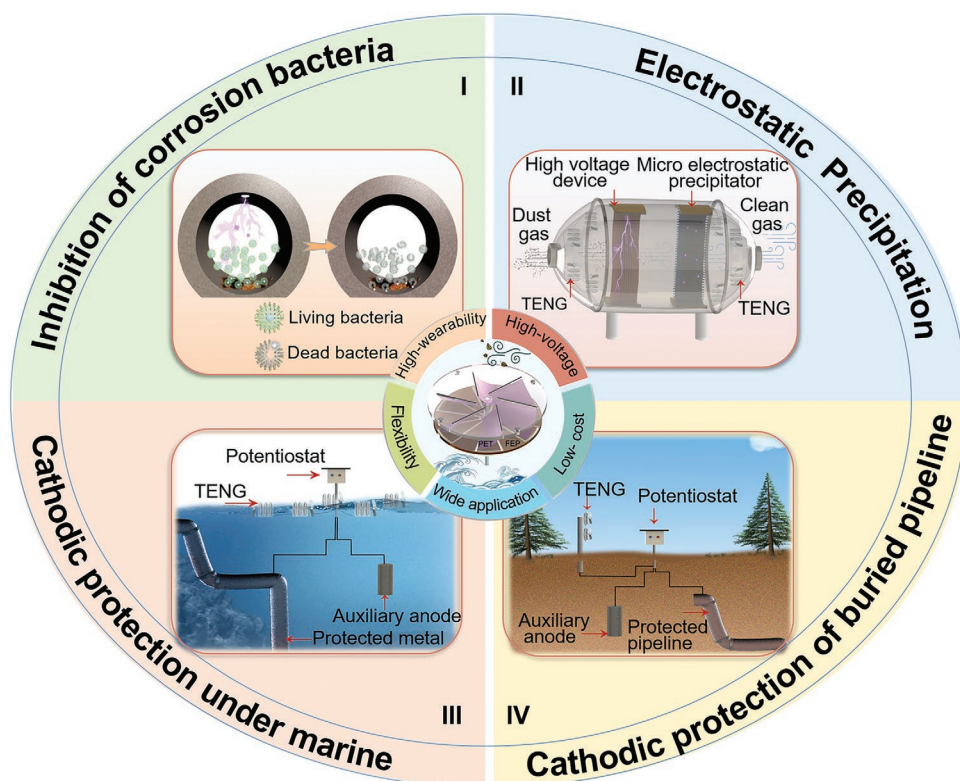


Figure 6. Prospective applications on the modified FR-TENG. (I) Inhibition of the corrosion bacteria based on the modified FR-TENG. (II) Electrostatic precipitation of chemical industry, through the high voltage device and micro electrostatic precipitator powered by the modified FR-TENGs. (III) ICCP of metal equipment in normal marine environments, powered by the modified FR-TENGs. (IV) ICCP of the buried pipelines at the soil, using the modified FR-TENGs as a power.

external conductor and the one electrode of grounding triboelectric nanogenerator, and not anymore be limited between the positive and the negative electrodes of TENG. Due to persistent spark discharge and arc discharge, the external grounding conductor could obtain electrical energy converted from mechanical energy.

Through the above systematic research, the output performance of FR-TENGs has increased remarkably, further expanding the application scenarios, especially in high-voltage applications. Due to its high output performance, this modified FR-TENG will play an effective role in the inhibition of microbial corrosion, high-voltage electrostatic dust removal scenarios, ICCP in marine environments and urban buried pipelines (Figure 6). Inspired by the high output voltage of this modified FR-TENG, it can apply a high-voltage electric field in the metal pipes that are being destroyed by corrosive bacteria, to inhibit the survival and reproduction of corrosive bacteria. This modified FR-TENG can also be applied to high-voltage electrostatic dust removal scenario. Collecting the mechanical energy of dusty gas during the treatment process, the modified FR-TENG can act as a high voltage generator and microelectrostatic device, effectively treating dust gas without using other energy sources. The dust in the gas charged by the high voltage generator and the microelectrostatic device, will be absorbed into the dust collector. The modified FR-TENG can collect ocean wave energy and wind energy, so it can be used as an external power source combined with a power management circuit, to apply ICCP for metal devices in the marine environment and buried pipelines which could reduce the corrosion potential of metal pipelines and inhibit corrosion phenomenon. This work not only presents the modified FR-TENG with ultrahigh voltage density that further expands the application scenarios, especially in high-voltage applications, but also could be regarded as guidance for the normalizing design of soft-contact FR-TENG.

Supporting Information

Supporting Information is available from the Wiley Online Library or from the author.

Acknowledgements

This work was supported by the National Key R & D Program of China under Grant No. 2016YFA0202703. The authors appreciate Xuelian Wei, Baocheng Wang for their assistance in writing this paper, and also Ruonan Li, Yanggui Sun, and Yating Peng for device fabrication and characterization analysis.

Conflict of Interest

The authors declare no conflict of interest.

Data Availability Statement

Research data are not shared.

Keywords

freestanding rotary TENGs, high-output performance, soft-contact, systematic research

Received: July 12, 2021

Revised: August 12, 2021

Published online:

- [1] C. A. Pizarro-Loaiza, A. Antón, M. Torrellas, P. Torres-Lozada, J. Palatsi, A. Bonmatí, *J. Cleaner Prod.* **2021**, 297, 126722.
- [2] S. Chu, A. J. N. Majumdar, *Nature* **2012**, 488, 294.
- [3] R. Best, R. Nepal, N. Saba, *J. Cleaner Prod.* **2021**, 297, 126618.
- [4] F. Fan, Z. Tian, Z. L. Wang, *Nano Energy* **2012**, 1, 328.
- [5] Z. L. Wang, *Nano Energy* **2019**, 58, 669.
- [6] Z. L. Wang, *Rep. Prog. Phys.* **2021**, <https://doi.org/10.1088/1361-6633/ac0a50>.
- [7] a) X. Liang, T. Jiang, Y. Feng, P. Lu, J. An, Z. L. Wang, *Adv. Energy Mater.* **2020**, 10, 2002123; b) Y. Li, M. Bouza, C. Wu, H. Guo, D. Huang, G. Doron, J. S. Temenoff, A. A. Stecenko, Z. L. Wang, F. M. Fernandez, *Nat. Commun.* **2020**, 11, 5625.
- [8] a) X. Peng, K. Dong, C. Ye, Y. Jiang, S. Zhai, R. Cheng, D. Liu, X. Gao, J. Wang, Z. L. Wang, *Sci. Adv.* **2020**, 6, 10; b) J. Wang, Z. Wu, L. Pan, R. Gao, B. Zhang, L. Yang, H. Guo, R. Liao, Z. L. Wang, *ACS Nano* **2019**, 13, 2587; c) Z. Wu, H. Guo, W. Ding, Y. Wang, L. Zhang, Z. L. Wang, *ACS Nano* **2019**, 13, 2349; d) H. Ouyang, Z. Liu, N. Li, B. Shi, Y. Zou, F. Xie, Y. Ma, Z. Li, H. Li, Q. Zheng, X. Qu, Y. Fan, Z. L. Wang, H. Zhang, Z. Li, *Nat. Commun.* **2019**, 10, 10.
- [9] a) M. Ma, Z. Zhang, Z. Zhao, Q. Liao, Z. Kang, F. Gao, X. Zhao, Y. Zhang, *Nano Energy* **2019**, 66, 104105; b) H. Guo, X. Pu, J. Chen, Y. Meng, M. H. Yeh, G. Liu, Q. Tang, B. Chen, D. Liu, S. Qi, C. Wu, C. Hu, J. Wang, Z. L. Wang, *Sci. Rob.* **2018**, 3, 2516; c) Z. Wu, T. Cheng, Z. L. Wang, *Sensors* **2020**, 20, 2925; d) R. Li, X. Wei, J. Xu, J. Chen, B. Li, Z. Wu, Z. L. Wang, *Micromachines* **2021**, 12, 352.
- [10] a) Z. L. Wang, *Nature* **2017**, 542, 159; b) Z. L. Wang, T. Jiang, L. Xu, *Nano Energy* **2017**, 39, 9.
- [11] a) J. Wang, Y. Zi, S. Li, X. Chen, *MRS Energy Sustainability* **2020**, 6, E17; b) R. Lei, Y. Shi, Y. Ding, J. Nie, S. Li, F. Wang, H. Zhai, X. Chen, Z. L. Wang, *Energy Environ. Sci.* **2020**, 13, 2178.
- [12] H. Guo, Z. Wen, Y. Zi, M.-H. Yeh, J. Wang, L. Zhu, C. Hu, Z. L. Wang, *Adv. Energy Mater.* **2016**, 6, 1501593.
- [13] a) M. Qi, R. Zhao, Q. Liu, H. Yan, Y. Zhang, S. Wang, Y. Yuan, *Food Control* **2021**, 120, 107566; b) K. Xia, J. Fu, Z. Xu, *Adv. Energy Mater.* **2020**, 10, 2000426; c) Z. Wang, Y. Shi, F. Liu, H. Wang, X. Liu, R. Sun, Y. Lu, L. Ji, Z. L. Wang, J. Cheng, *Nano Energy* **2020**, 74, 104910; d) H. Guo, J. Chen, L. Wang, A. Wang, Y. Li, C. An, J. He, C. Hu, V. K. S. Hsiao, Z. L. Wang, *Nat. Sustainability* **2021**, 4, 147.
- [14] L. Lin, S. Wang, Y. Xie, Q. Jing, S. Niu, Y. Hu, Z. L. Wang, *Nano Lett.* **2013**, 13, 2916.
- [15] a) G. Zhu, J. Chen, T. Zhang, Q. Jing, Z. L. Wang, *Nat. Commun.* **2014**, 5, 9; b) G. Cheng, Z. Lin, Z. Du, Z. L. Wang, *ACS Nano* **2014**, 8, 1932.
- [16] a) S. Chen, N. Wang, L. Ma, T. Li, M. Willander, Y. Jie, X. Cao, Z. L. Wang, *Adv. Energy Mater.* **2016**, 6, 9; b) Z. Lin, B. Zhang, H. Zou, Z. Wu, H. Guo, Y. Zhang, J. Yang, Z. L. Wang, *Nano Energy* **2020**, 68, 104378; c) N. Zhai, Z. Wen, X. Chen, A. Wei, M. Sha, J. Fu, Y. Liu, J. Zhong, X. Sun, *Adv. Energy Mater.* **2020**, 10, 9; d) Y. Bai, L. Xu, C. He, L. Zhu, X. Yang, T. Jiang, J. Nie, W. Zhong, Z. L. Wang, *Nano Energy* **2019**, 66, 104117; e) X. Wei, Z. Wen, Y. Liu, N. Zhai, A. Wei, K. Feng, G. Yuan, J. Zhong, Y. Qiang, X. Sun, *Nano-Micro Lett.* **2020**, 12, 88.
- [17] P. Wang, L. Pan, J. Wang, M. Xu, G. Dai, H. Zou, K. Dong, Z. L. Wang, *ACS Nano* **2018**, 12, 9433.
- [18] a) J. Cheng, W. Ding, Y. Zi, Y. Lu, L. Ji, F. Liu, C. Wu, Z. L. Wang, *Nat. Commun.* **2018**, 9, 3733; b) Y. Zhong, H. Zhao, Y. Guo, P. Rui,

- S. Shi, W. Zhang, Y. Liao, P. Wang, Z. L. Wang, *Adv. Mater. Technol.* **2019**, *4*, 1900741.
- [19] a) W. Yang, Y. Wang, Y. Li, J. Wang, T. Cheng, Z. L. Wang, *Nano Energy* **2019**, *66*, 104104; b) X. Li, X. Yin, Z. Zhao, L. Zhou, D. Liu, C. Zhang, C. Zhang, W. Zhang, S. Li, J. Wang, Z. L. Wang, *Adv. Energy Mater.* **2020**, *10*, 1903024; c) C. Zhang, Y. Liu, B. Zhang, O. Yang, W. Yuan, L. He, X. Wei, J. Wang, Z. L. Wang, *ACS Energy Lett.* **2021**, *6*, 1490.
- [20] H. Zou, Y. Zhang, L. Guo, P. Wang, X. He, G. Dai, H. Zheng, C. Chen, A. C. Wang, C. Xu, Z. L. Wang, *Nat. Commun.* **2019**, *10*, 1427.
- [21] a) Z. L. Wang, *Mater. Today* **2017**, *20*, 74; b) S. Niu, Z. L. Wang, *Nano Energy* **2015**, *14*, 161.
- [22] Y. Liu, J. Mo, Q. Fu, Y. Lu, N. Zhang, S. Wang, S. Nie, *Adv. Funct. Mater.* **2020**, *30*, 2004714.
- [23] a) S.-H. Shin, Y. H. Kwon, Y.-H. Kim, J.-Y. Jung, M. H. Lee, J. Nah, *ACS Nano* **2015**, *9*, 4621; b) S. H. Shin, Y. E. Bae, H. K. Moon, J. Kim, S. H. Choi, Y. Kim, H. J. Yoon, M. H. Lee, J. Nah, *ACS Nano* **2017**, *11*, 6131; c) S. Wang, Y. Zi, Y. Zhou, S. Li, F. Fan, L. Lin, Z. L. Wang, *J. Mater. Chem. A* **2016**, *4*, 3728.
- [24] H. Amii, K. Uneyama, *Chem. Rev.* **2009**, *109*, 2119.